CRYSTAL GROWTH & DESIGN

pubs.acs.org/crystal

Article

Effect of Heating on Avian (Cortical and Medullary) Bone Chemistry, Mineralogy and Structural Organization

Alejandro B. Rodríguez Navarro,* Sergio Madero, Martina Greiner, Pablo A. Rodriguez-Jimenez, Wolfgang W. Schmahl, and Concepción Jiménez-López

Cite This: https://doi.org/10.1021/acs.cgd.3c00648

Read Online

ACCESS | Metrics & More | Article Recommendations | Supporting Information

ABSTRACT: The study of bone changes induced by heating is highly relevant for forensic and archeological analyses as well as for the production of bone-derived materials with novel properties and applications. In the present study, we study in detail how different types of avian bone (cortical, medullary) transform during thermal treatments (up to 800 °C) using different analytical techniques such as thermogravimetry (TGA-DSC), electron microscopy, X-ray diffraction and infrared spectroscopy. We show that bone transformation following thermal treatments is strongly influenced by bone architecture, the composition of the organic matrix, and the integration of the mineral with the organic fractions. For instance, in avian cortical bone, the apatite nanocrystals are integrated within collagen fibrils and coated with phosphorylated proteins. During heating, the collagen losses structural order and denatures (at around 200 °C), losing all structural integrity at 300 °C. In the bone mineral fraction, there is a gradual conversion of phosphate, in poorly crystalline/amorphous environments, into apatite (up to 400 °C). However, it is not until all organics are completely lost at around 600 °C that recrystallization sets in with a rapid increase in the size of apatite crystals. Also, during recrystallization, foreign ions (Mg^{2+}, Na^{+}) are expelled from the apatite lattice to the crystal surface, and the degree of preferential orientation of the apatite crystals increases as larger, well-oriented apatite crystals grow epitaxially at the expense of smaller, randomly oriented crystals. However, the scenario is different for the medullary bone. In this case, with an organic matrix rich in noncollagen proteins and proteoglycans, the recrystallization sets in at much lower temperatures (around 400 °C compared to 600 °C in cortical bone). Thus, the association of mineral and organic components controls recrystallization, particularly in the case of apatite nanocrystals within collagen fibrils in cortical bone. Also, the calcination process creates additional microporosity in both types of bone, increasing the bone mineral surface area and reactivity. The information obtained in this study provides a better understanding of the dynamics of bone transformation during alteration in natural processes (e.g., diagenesis, burning) and how bone mineral characteristics can be modified for specific applications (e.g., bone grafts, waste removal, or chromatography).

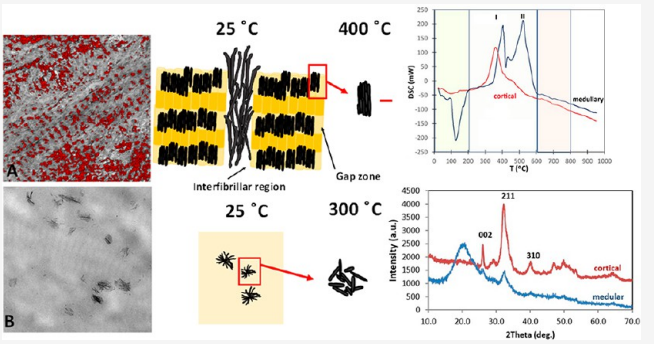

INTRODUCTION

Following heating, bone experiences extensive changes in its chemical composition, structure, and mineralogy. The understanding of those changes is highly relevant in a wide range of areas, going from Forensic Science and Archaeology (to identify the conditions at which bones were exposed) to Material Science (to obtain bone-derived materials with novel properties and applications).[1−8] Also, understanding heat-induced changes in bones is relevant in biotechnological processes such as the production of hydroxyapatite materials for bone implants or grafts or for environmental remediation.[5,9−11] For instance, deproteinate bone mineral produced by thermal treatments can be used as safe and biocompatible fillers, cements, or grafts for bone regeneration. Moreover, heating preserves some of the chemical and structural characteristics of natural bone and generates additional porosity that facilitates osseointegration.[12] Also, the high capacity for elemental substitution of apatite structure, and the large surface area of bone mineral, can be used for the removal of heavy metals from contaminated sites or for protein chromatography.[11] Therefore, understanding heat-induced changes is critical to controlling the properties of these bone derived materials.

Bone is a composite material with a complex chemical composition and hierarchical structure that serves different

Received: May 26, 2023
Revised: September 21, 2023

functions, such as structural support and supply of ions for homeostasis.[13−15] Bone is composed of an inorganic phase (carbonated apatite nanocrystals) mineralizing an organic matrix (largely type I collagen) and water. Type I collagen molecules self-assemble into a triple helix structure stabilized by hydrogen bonds bridging adjacent molecules. Collagen microfibrils have a characteristic banding pattern (with 67 nm repeats) produced by a 40 nm gap zone between the ends of the individual collagen molecules, and a 27 nm region in which they overlap.[16] Apatite nanocrystals, mineralizing collagen, nucleate within the gap zones, on the fibrils surface and in the interfibrillar space.[16−18] Besides collagen, there are a large number of noncollagenous phosphoproteins (NCPs) (i.e., osteocalcin, osteopontin), strongly bound to the apatite crystal surface, that play an important role controlling the nucleation and growth of apatite, as well as its attachment to collagen.[4,19−23] The integration of the mineral within the organics reduces mineral reactivity and solubility, and controls the recrystallization induced by diagenesis or by heating.[4,7,24]

However, bone composition and structure are highly heterogeneous and vary with age and location in the skeleton depending on bone function.[25,26] It is also a living tissue that is constantly accreted and remodeled by bone cells, so its properties change overtime.[14] Given the heterogeneous composition and complex structure of bone, there is not a complete understanding of how bone transforms with heating and what factors control this process. This is crucial to better understand alteration processes occurring in archeological bone during heating, burying, and/or diagenesis, or how to control bone-derived materials' properties for implants or other applications.[3−5,10,11]

Here, we study in detail the changes occurring in bone induced by thermal heating. In particular, to understand how the mineral characteristics, the composition of the organic fraction, and the association of mineral−organics influence the transformation, we used cortical and medullary bone from long bones of laying hens, which represent two types of bone tissues with very different organic matrix composition, organization and mineral properties.[27−29] Cortical bone is a dense structural bone that forms a cortex surrounding the marrow cavity. The basic structural units are collagen fibrils mineralized by carbonate apatite nanocrystals oriented with their *c*-axis parallel to the fibrils. The tissue is organized into cylindrical structural units (osteons) surrounding a central canal, the Haversian canal, responsible for transporting the blood vessels and nerves.[14] On the other hand, medullary bone is a special type of bone formed within the marrow cavities of long bones of female birds during reproduction, that is highly reactive and metabolically active as it acts as a labile source of calcium for rapid eggshell calcification.[29−31] Medullary bone consists of apatite nanocrystals of very small size deposited randomly in an organic matrix rich in proteoglycans.[27,28,32] The low crystallinity and high carbonate content could explain the extremely high reactivity and the solubility of medullary bone mineral, which is at least 30-fold greater than that of cortical bone.[24]

To follow the changes that occur in the chemical composition and structural organization of the different types of bones during the heating process, we used complementary analytical techniques such as thermogravimetric analysis and electron microscopy, infrared spectroscopy, and X-ray diffraction. The information obtained in this study can help to better understand the dynamics of bone alteration processes.

MATERIALS AND METHODS

2.1. Bone Samples. Tibiae samples from White Leghorn laying hens (65 weeks old) were selected for this study. The experimental and raising condition of these animals is fully described elsewhere.[33] Bone samples were kept in a freezer (−20 °C). One-centimeter-thick slices were cut from each tibia at mid-diaphysis to prepare longitudinal pieces of cortical bone (about 10 mm × 5 mm × 0.5 mm in size) and to extract the medullary bone (>10 g) from the marrow cavity. The cortical and medullary bone from the tibiae mid-diaphysis were manually separated using a scalpel. Medullary bone collected from several bones was homogenized.

2.2. Heating Experiments. To study the process of bone transformation with heating, pieces of cortical bone and homogenized medullary bone were annealed at different temperatures (from 100 °C until 800 °C in 100 °C intervals) for 1 h in air in a Carbolite furnace (model 1100). Samples were placed in a crucible and inserted in the furnace at the preset temperature. They were removed after 60 min and left to cool down at room temperature. To study the organic bone matrix, bone samples were demineralized by immersing them in 1% HCl solution under shaking overnight. Demineralized samples were rinsed twice with milli-Q water to remove any residual HCl, then dried at room temperature for 24 h.

2.3. Electron Microscopy. Scanning electron microscopy (SEM) observation was carried out on polished cross sections of the tibiae mid-diaphyses. To prepare the sections, bone samples were fixed with 4% glutaraldehyde, embedded in Epothin epoxy resin (Buehler), cut, polished, coated with carbon (Hitachi UHS evaporator), and observed with a variable pressure SEM (LEO 1430-VP) using a backscattering electron (BSE) detector and an accelerating voltage of 30 keV. A selection of bone samples from each temperature was analyzed by transmission electron microscopy (TEM). Untreated bone samples (25 °C) were fixed with 2.5% glutaraldehyde and cacodylate buffer (0.1 M, pH = 7.4) for 4 h at 4 °C. Later on, samples were dehydrated using an ethanol gradient (50, 70, 90, and 100%), and embedded in Spurr epoxy resin. Then, they were ultrathinly sectioned (50−70 nm thick) with a LEICA Ultracut R (Germany), carbon coated, and analyzed using a Carl Zeiss LIBRA 120 PLUS (Germany) TEM microscope equipped with an EELS (Electron Energy Loss Spectroscopy) detector or a Thermo-Fisher TALOS F200 XTEM (USA) equipped with a EDX detector. EELS was used to map the Ca distribution and EDX other elements. Bone treated at different temperatures (200 °C and above) were grounded, and fine particles were suspended in ethanol, fished with a TEM grid, and observed with the TALOS TEM system.

2.5. Infrared Spectrometry and Thermogravimetry. To follow the changes in chemical composition of bone tissues (cortical and medullary bone) during heating, bone samples in powder form were analyzed using an ATR system (MIRacle Single Reflection ATR, PIKE Technologies), and the infrared spectra were recorded at a 2 cm^{-1} resolution over 40 scans using an FTIR spectrometer (model 6600, JASCO Analytical Instruments Japan). The composition was analyzed using the absorption bands associated with the characteristic molecular groups of each component (e.g., O−H: water; C−H: lipids; amide I: collagen; ν_2, ν_3 CO_3: carbonates; ν_1, ν_3 PO_4: phosphates).[29] The FTIR spectra were deconvoluted to resolve overlapping peaks from different molecular groups using PeakFit v. 4.12 software (Seasolve, USA), and their peak areas calculated, as described in more detail in the Supporting Information (Figure S5).

The relative amounts of water, organic matter, phosphate, and carbonate in the bone samples were determined by thermogravimetric analysis using approximately 30 mg of each sample and a TGA system from METTLER-TOLEDO (model TGA/DSC1). A heating rate of 20 °C/min in air was used for registering the TGA curves.

2.6. X-ray Diffraction. The mineralogy and microstructure of bone samples were analyzed by powder X-ray diffraction. Bone samples in powder form were analyzed with a Panalytical Xpert Pro X-ray powder diffractometer (Panalytical Xpert Pro, Almelo, The Netherlands) operating in reflection mode using copper radiation to determine Theta-2Theta scans (from 4 to 120° with 0.017° step size

https://doi.org/10.1021/acs.cgd.3c00648
Cryst. Growth Des. XXXX, XXX, XXX−XXX

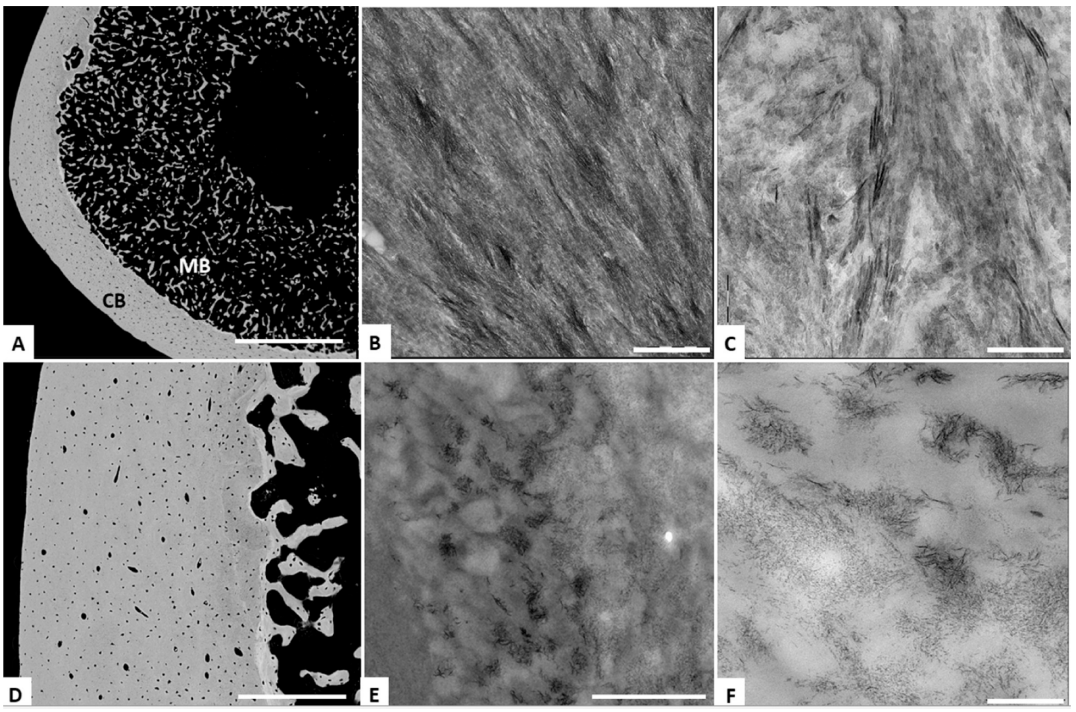

Figure 1. Electron microscopy of (untreated) bone. A) SEM images of a tibia cross-section showing cortical bone (CB) and medullary bone (MB) partially filling the marrow cavity. B) Highly oriented and mineralized collagen fibrils in cortical bone, as seen by TEM. C) TEM images of elongated apatite crystals within collagen fibrils. D) Detail of cortical bone showing osteons around Harversian canals and medullary trabecula with osteocytes close to the inner cortex (endosteal) surface. E, F) TEM images of aggregates of apatite crystals mineralizing the medullary bone matrix. Scale bars: A) 1 mm; B) 500 nm; C) 200 nm; D) 200 μm; E) 1 μm; and F) 200 nm.

and 100 s integration time per step). Analyses of XRD profiles were done using TOPAS 5.0 software (Bruker, Karlsruhe, Germany). To determine the crystallite size of apatite crystals, apatite reflections were fitted using a Peak phase model, and the crystallite size along the *c*-axis and *a*-axis were determined from 002 and 310 reflections using the Scherrer method and a K value of 0.9. For 2D X-ray diffraction, pieces of tibiae cortical bone (about 10 mm × 5 mm in size), cut longitudinally from the midshaft of the diaphysis, were analyzed in transmission mode with an X-ray single crystal diffractometer equipped with a PHOTON area detector (D8 Venture, Bruker, Germany) and a dual microsource (Cu and Mo). A 0.2 mm collimated beam, 120 s of exposure time, and Mo radiation were used. Each sample was measured at three different points separated by 1 mm. For the analysis of organic matter extracted from demineralized bone samples, a Cu microsource was used. A quantitative estimation of the degree of alignment of the *c*-axis of apatite crystals in the cortical bone was determined from the angular breadth of bands displayed in the intensity profile along the Debye−Scherrer ring associated with the 002 reflection of the apatite mineral (Gamma scan).[29] For pole figures, samples were measured in reflection mode (2Theta = 20° and Omega = 10°), and a sequence of 2D patterns (72) were collected during a Phi scan with 5° steps. Crystallinity of bone mineral from different populations (oriented and nonoriented) was determined from 2D XRD data by measuring the full width at half-maximum (fwhm) of the main apatite peaks (e.g., 002, 211, 310) displayed in the calculated 2Theta scans (calculated by radially integrating intensities) and by applying the Scherrer formula. The sharper the peaks and the smaller the fwhm, the greater the crystallinity. XRD2DScan software v 8.0 (PANalytical, The Netherlands) was used to analyze the collected 2D X-ray diffraction patterns.

RESULTS AND DISCUSSION

Untreated Bone. Figure 1 shows representative electron microscopy images of avian bone (tibia) structure at the micro- and nanoscale. The tibia in the cross-section has an outer dense cortex (cortical bone; 0.5 mm thick) and a hollow cavity (the marrow or medullar cavity) that is partially filled with medullary bone, mostly near the endosteal surfaces (Figure 1A, D). Cortical bone is made of cylindrical structural units, or osteons, with osteocytes (embedded bone cells, seen as small pores) that are distributed around a central canal (e.g., Haversian channels), where blood vessels and nerves run (Figure 1D). The medullary bone consists of small, isolated trabeculae elements, that also contain osteocytes, and that are generally surrounded by a large number of osteoclasts and/or osteoblasts,[34] as they have a very fast remodeling rate to supply calcium needed for the eggshell formation.

The structures of cortical and medullary bone are very different at the nanoscale. Cortical bone is made of cross-linked collagen fibrils mineralized by apatite nanocrystals, that nucleate in the gap zones of the fibrils with a 67 nm repeat (Figures 1B, S1). Apatite crystals are elongated along the *c*-axis (about 22 nm × 5 nm in size) and are typically oriented parallel to the collagen fibrils (Figure 1C). Medullary bone has a small amount of collagen and, unlike in cortical bone, collagen fibrils are randomly oriented. Medullary bone extracellular organic matrix contains mainly proteoglycans, glycoproteins and noncollagenous proteins.[28,30] The different chemical composition of the organic matrix in these two types of bone causes them to stain differently.[34] The organic matrix is mineralized by aggregates of randomly oriented apatite nanocrystals, reminiscent of those found at early stages of (woven) bone mineralization[27,28] (Figures 1E, 1F, S2). Apatite crystals in medullary bone are also elongated along the *c*-axis but are smaller (about 15 nm × 2 nm; Figure S2). The small crystal size and large amount of carbonate substitutions make the mineral less stable and more soluble, facilitating mineral

https://doi.org/10.1021/acs.cgd.3c00648
Cryst. Growth Des. XXXX, XXX, XXX−XXX

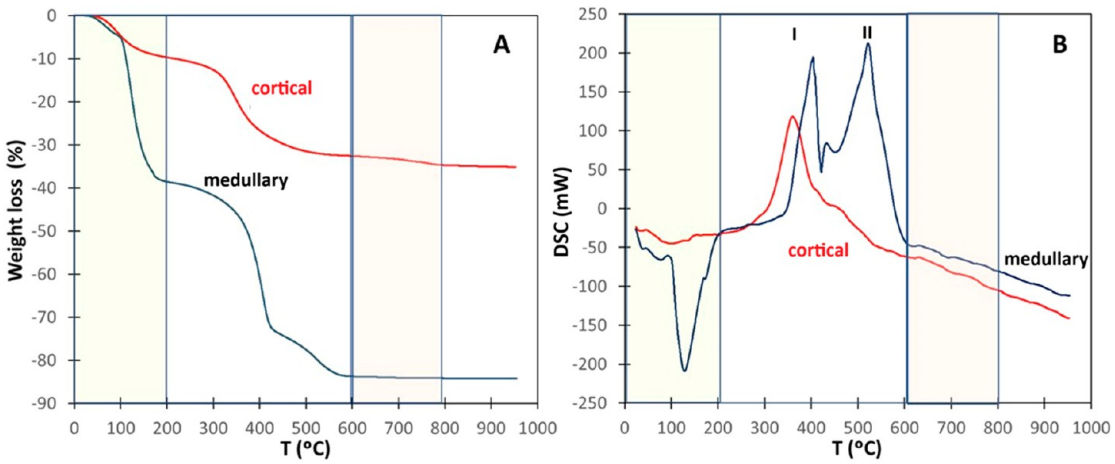

Figure 2. Thermogravimetric analysis (TGA-DSC) of bone. A) Representative TGA curves from cortical (red) and medullary (blue) bone displaying characteristic weight loss events occurring during heating, which correspond to water evaporation (25−200 °C), organic matter combustion (200−600 °C), and carbonate thermal decomposition and release of CO_2 (600−800 °C). B) DSC curves showing peaks from the heat absorbed (negative peak) or released (positive peak) during heating that are associated with previous weight loss events. Peaks I and II are associated with collagen, or NCPs, and proteoglycans, respectively.

dissolution.[24] Additionally, medullary bone trabeculae elements are generally surrounded by a large number of osteoclasts and/or osteoblasts,[34] which induce medullary bone mineralization/demineralization during the egg laying daily cycle.

Effect of Heating. The observed changes in bone chemistry and structure during heating reproduces well some of the results obtained by other authors,[1,2,5,7,8,35] and, in addition, our results show how the mineral transforms with heating and reorganizes during the recrystallization, changing its crystallographic orientation and surface chemistry, as described below. Moreover, it is shown how the different organic matrix composition of the two types of bone studied and the mineral-organic matrix association determine these transformations.

The most evident change in bone induced by heating is a color change due to the combustion of organic components and char formation. With increasing temperature, bone color changes from a brownish caramel color at 200−300 °C, a gray to black color from 400 to 500 °C, and from a gray to a white color at 600 °C and above. The macroscopic appearance and color of archeological bones offer a first estimation of the temperature at which bone were exposed. However, other factors such as the duration of the thermal exposure and oxygen availability strongly influence these changes.[1,7,8]

Although the original external shape and volume of bone are well preserved up to at least 800 °C, bone chemical composition changes extensively with temperature due to dehydration and loss of the different components (organics, carbonate). These compositional changes were analyzed by thermogravimetry and differential scanning calorimetry (TGA-DSC). TGA graphs show three main weight loss events (Figure 2): 1) 25−200 °C (water loss); 2) 200−600 °C (organic matter combustion); and 3) 600−800 °C (thermal decomposition of carbonates and release of CO_2) (Figure 2A). The weight lost in each step is different for the two types of bones studied, as they have different chemical composition. The ash weight or amount of remnant mineral at 600 °C in cortical bone is always higher (about 65% of the original bone) than that of medullary bone (about 30−35%). Although cortical and medullary bone particles display similar brightness in the SEM (back scattering imaging mode; Figures 1A, 1D), differences in ash weight and thermal behavior could be explained, on one hand, by the presence of marrow organic matter and, on the other, by a different carbonate content in the mineral fraction [greater in medullary bone than in cortical bone (about 11% and 7%, respectively[26])].

The different compositions of cortical and medullary bone organic matrices can also be argued to explain differences in DSC data (Figure 2B). While cortical bone shows a single large exothermic peak at around 390 °C, medullary bone shows two exothermic peaks: a smaller one at about 400 °C and a larger one at about 500 °C (Figure 2B). The peak of cortical bone and the first peak of medullary bone could be attributed to the thermal decomposition of collagen and noncollagenous proteins (NCPs), and the second peak in medullary bone should be attributed to the thermal decomposition of proteoglycans, which are the major components of the organic matrix in this type of bone. Proteoglycans are thermally more stable than proteins (such as collagen) and decompose at higher temperatures.[36−38]

Infrared Spectroscopy. Infrared spectroscopy is very informative and sensitive to the changes occurring in bone chemistry and structure during heating due to dehydration, loss of organic components (lipids and collagen), and recrystallization of the mineral. FTIR spectra of cortical and medullary bone (Figure 3) shows identical infrared absorption bands (i.e., CH bands from polysaccharides and lipids, amide bands from bone collagen, phosphate and carbonate bands from bone mineral), though their relative intensities change as both tissues have different chemical composition. In fact, medullary bone has more intense methyl (CH) peaks (around 2900 cm^{-1}) and carbonyl (C═O) peaks (around 1740 cm^{-1}) from polysaccharides and lipids, and less intense ν_1, ν_3 PO_4 and ν_2, ν_3 CO_3 bands from the mineral part (phosphate and carbonate). Thus, these data show that the organic matrix of medullary bone contains a larger amount of lipids and polysaccharides and has a lower degree of mineralization than cortical bone. These results are in agreement with those observed from TGA analyses (Figure 2A).

In the context of heating effects, up to 200 °C, there are only minor changes in the infrared spectra for both types of bones

https://doi.org/10.1021/acs.cgd.3c00648
Cryst. Growth Des. XXXX, XXX, XXX−XXX

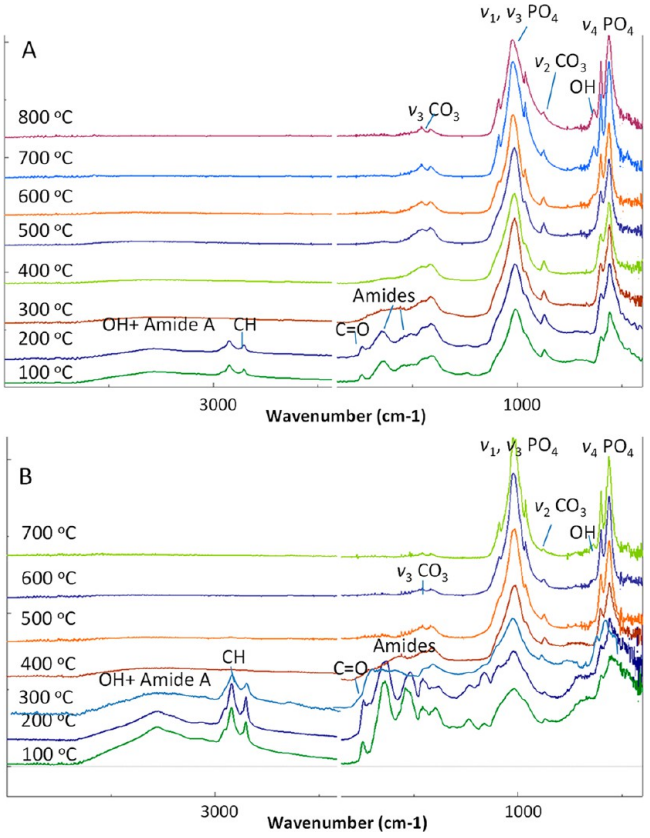

Figure 3. FTIR spectra of bone treated at different temperatures. A) Cortical bone. B) Medullary bone. Main molecular groups of the bone organic matrix and bone mineral detected by IR spectroscopy are indicated.

(Figures 3, S6, S7), mainly consisting of a reduction of the intensity of the OH band (around 3000−3500 cm^{-1}) due to the loss of water (Figure S6A). At 300 °C, the methyl (CH) peaks (near 2920 cm^{-1}) and carbonyl (C═O) peaks are no longer detectable due to the loss of lipids. At 400 °C, there is a marked reduction in amide peak intensity accompanied by a notable peak broadening (individual amide peaks are no longer resolved), due to the thermal degradation of collagen in cortical bone and NCPs in medullary bone. At 500 °C, the amide peaks have disappeared. At 600 °C and an above, there is a notable reduction of the intensity of the main carbonate band (around 1410 cm^{-1}) associated with type B carbonate. At the same time, above 400 °C, the peak area ratio between carbonate peaks at 1450 cm^{-1} (associated with type A carbonate) and 1405 cm^{-1} (associated with type A carbonate) increases, indicating that there is a gradual mobilization of carbonate from type B to type A sites in the apatite structure (Figure S6C). On the other hand, with increasing temperature (>400 °C), there is a gradual sharpening and splitting in phosphate bands due to an increased apatite crystallinity during recrystallization. These results reproduce those from other authors studying the aerobic combustion of bone.[5,7,8] Also, up to 400 °C, the relative intensity of phosphate subbands in the ν_4 PO$_4$ domain[39] changes with temperature (Figure S6D): the intensity of the band at 539 cm^{-1} (associated with acid phosphate HPO_4^{2-}) decreases, and the intensity of the band at 600 cm^{-1} (associated with apatitic PO$_4$) increases, indicating that phosphate in poorly crystalline or amorphous environments is converting into highly crystalline apatitic phosphate. In bone apatite nanoparticles, it has been proposed that there is an amorphous or poorly crystalline external hydrated layer rich in carbonate and acid phosphate surrounding a crystalline apatite core.[40] With heating and after dehydratation (>200 °C), this layer crystallizes (as observed in our experiments with the loss of nonapatitic phosphate bands; see Figure S6D). The existence of poorly crystalline or amorphous components in bone mineral, that are progressively converting into crystalline components, is in agreement with current models of bone mineral forming from amorphous precursors (i.e., amorphous calcium phosphate) or how bone mineral crystallinity changes during maturation and/or remodeling.[25,40,41]

Above 600 °C, a peak at 630 cm^{-1} and a smaller peak at 3600 cm^{-1} started to appear. These peaks are associated with OH^- ions replacing carbonate groups (type A) in the apatite structure, indicating that bone mineral is converting into hydroxylapatite.[7] These results are in agreement with other studies[7,8] showing that bone apatite structure has a high capacity to exchange ions between different structural sites, and that such ionic mobility increases with temperature.[42]

Regarding the bone organic matrix, though no notable changes in infrared spectra were observed up to 200 °C, there are relevant changes in collagen structure, even at lower temperatures. For instance, Kubisz[43] and Ferreira et al.[44] have shown that bone collagen denaturalization occurs between 130 and 180 °C, when the structure of collagen changes from an α-helix to a random coil, due to the release of bound water that stabilizes the structure. However, other authors[45] show that collagen conformational changes and degradation in mineralized bone occur at higher temperatures (between 237 and 327 °C). This discrepancy could be understood if the collagen−mineral interaction is considered, as the mineral protects the collagen and delays its degradation. Our data align to this idea, as complete thermal degradation of collagen and/or by-products was observed at ∼390 °C, associated with a main weight loss event and a large exothermic peak in TGA-DSC graphs (Figure 2), which could be induced by the combustion of amino acids and the subsequent release of NH_3 and NO_2.[7] Above 600 °C, more notable changes occur in the mineral part of the bone, with ionic exchange between structural sites in the crystal lattice and a gradual increase in crystallinity.

Electron Microscopy: Bone Microstructure. The loss of organic components and mineral recrystallization during heating also generate important changes in bone microstructure, as revealed by electron microscopy. In cortical bone, the organization of the mineral is very well preserved, at least up to 800 °C. Figure 4A shows that the surface of the bone treated at 400 °C is quite smooth. However, at higher magnification, the surface shows bundles of fibrils running parallel to the elongation of bone and that are partially covered by organic membranes. Each bundle is formed by densely packed mineralized fibrils which are highly aligned. In bone treated at 800 °C, the bundles are fully exposed and apatite nanoparticles have recrystallized, forming strings of crystals about 80 nm in diameter (Figure 4D−4F).

Medullary bone treated at high temperatures has a highly porous structure as all the organic matter has been removed, and only the mineral part is left (Figure 4G). The mineral part is made of isolated trabeculae a few tens of microns in size with a very irregular shape and rough surface. They are made of apatite nanocrystals fused together into aggregates about 200

https://doi.org/10.1021/acs.cgd.3c00648
Cryst. Growth Des. XXXX, XXX, XXX−XXX

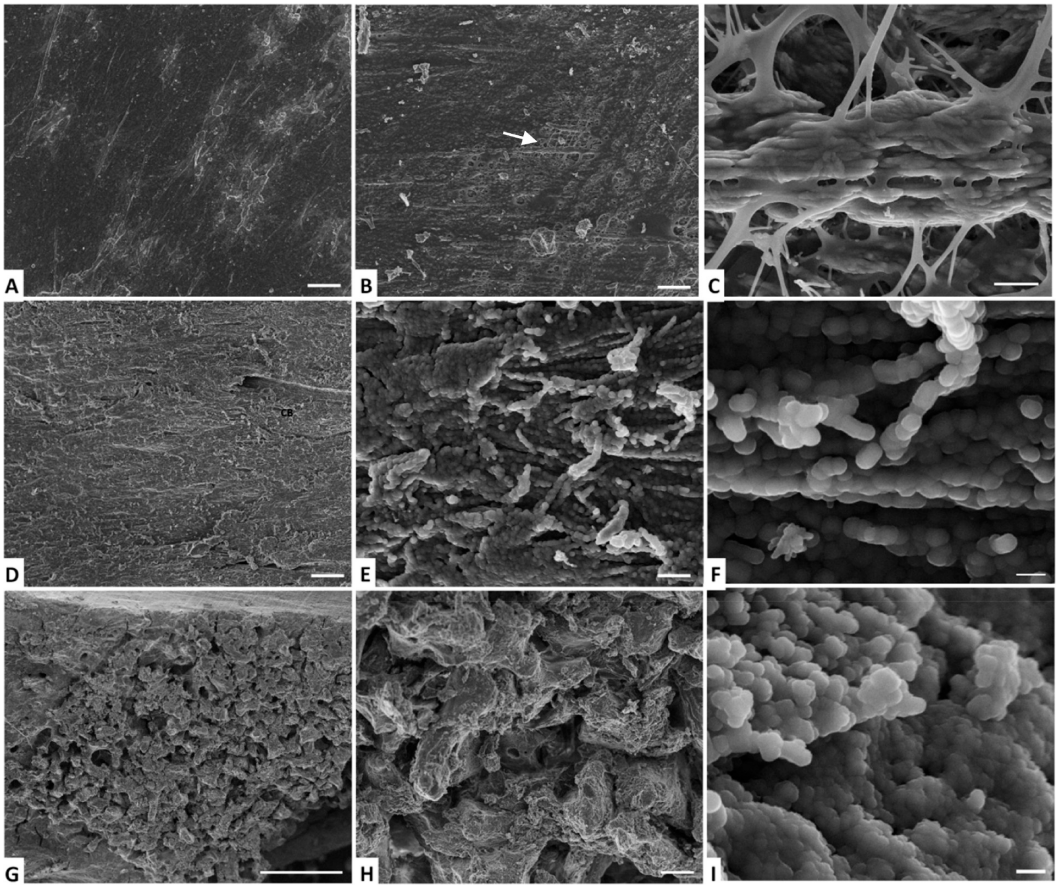

Figure 4. Evolution of bone microstructure with temperature analyzed by scanning electron microscopy. A−C) Imaging of cortical bone treated at 400 °C showing bundles of mineralized collagen fibrils running parallel to the elongation of bone (horizontal direction; see arrow). D−F) Cortical bone treated at 800 °C showing bundles of recrystallized apatite particles arranged in well-ordered parallel arrays. G−I) Imaging of medullary bone treated at 800 °C showing a highly porous structure made of mineral trabeculae. Each trabecula is made of a massive aggregate of nanoapatite crystals. Scale bars: A: 100 μm; B, 10 μm; C, 1 μm; D, 10 μm; E, 1 μm; F, 100 nm; G, 100 μm; H, 10 μm; and I, 100 nm.

nm in size that are formed during recrystallization (Figure 4H, 4I).

Electron Microscopy: Bone Nanostructure. TEM observation of tibiae cortical and medullary bone samples treated at different temperatures (annealing for 1 h) shows that heating has also induced notable changes in bone structure at the nanoscale. In cortical bone, the organization of the mineral is very well preserved, at least up to 500 °C. Figures 5A and S3 show packages of highly aligned apatite crystals that have imprinted the periodic banding of the collagen fibrils in which they mineralized (seen as slight changes in electron density). TEM images show that the size of apatite crystals is nearly constant up to 400 °C (22 nm × 5 nm) and increases slowly first up to 600 °C (60 nm × 9 nm) and very rapidly at higher temperatures, adopting a nearly rounded morphology at 700 °C (250 nm in diameter) and a euhedral crystal morphology at 800 °C (400 nm in diameter) (Figures 5A−5C). The increase in the size of crystals is due to a recrystallization process in the solid state, in which smaller crystals coalesce and/or provide material, through diffusion, for the growth of larger crystals at the expense of smaller ones (Oswald ripening).[9,46]

In medullary bone, the recrystallization process starts earlier (at about 400 °C), and the crystal size increases faster than that in cortical bone (Figures 4, 5, and S4). Crystal size increases from 26 nm × 4 nm at 400 °C, to 85 nm × 27 nm at 500 °C, and 120 nm in diameter at 600 °C. It seems that the growth of bone apatite crystals is constrained, especially in their width, up to this temperature. However, at temperatures >600 °C, when the organic components (i.e., collagen, proteins) and their decomposition products are lost, the crystals grow uninhibited in all directions (length and width), developing a rounded morphology above 700 °C (see Figure 5E, 5F). A schematic drawing is presented in Figure 6, which illustrates the changes induced by heating during the recrystallization process of minerals in cortical and medullary bone.

In order to understand these changes, the composition of the organics present in the different type of bones and the interaction mineral−organics must be taken into account. Many noncollagenous proteins (NCPs) are phosphoproteins (i.e., osteocalcin, osteopontin), which are strongly bound to apatite crystal surfaces and, as such, play an important role controlling the nucleation and growth of apatite.[4,16,19,20,22] In both types of bone, apatite crystals are elongated along the *c*-axis. This could be explained by the preferential attachment of acidic proteins (i.e., osteocalcin) to (100) faces, arresting their growth and resulting in the elongated shape of apatite crystals in bone.[47] These proteins may also facilitate the attachment of apatite crystals to collagen and determine the typical parallel orientation of apatite to the collagen fibrils (in cortical bone). These proteins can also control recrystallization, as crystal growth is inhibited until all organics coating the crystal surfaces

https://doi.org/10.1021/acs.cgd.3c00648
Cryst. Growth Des. XXXX, XXX, XXX−XXX

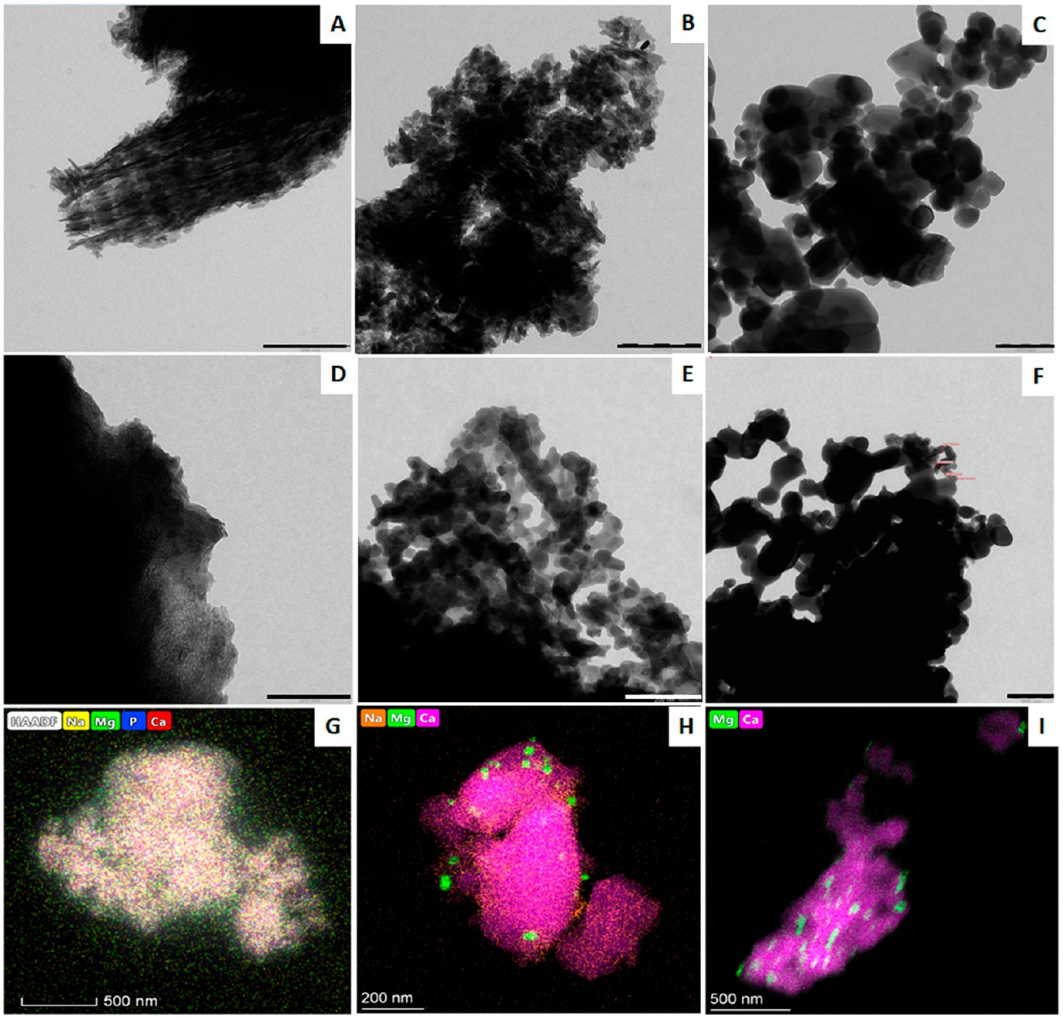

Figure 5. Evolution of bone nanostructure with temperature analyzed by transmission electron microscopy. A) Cortical bone treated at 500 °C showing the banding pattern of preexisting collagen. B) cortical bone treated at 600 °C. C) cortical bone treated at 800 °C showing recrystallized apatite particles. D–F) Imaging of medullary bone treated at 400 °C (D), 500 °C (E), and 700 °C (F). G–I) Elemental mapping of bone particles analyzed by EDS showing the distribution of Ca and Mg. Cortical bone treated at 600 °C (G) and at 800 °C (H). I) Medullary bone treated at 800 °C. Scale bars: A–F) 200 nm.

are completely removed and crystals grow unhindered in all directions, developing rounded and then well-faceted morphologies.[5,7,16] Interestingly, even though the main organic matrix components of cortical bone (collagen, NCP) are less thermally stable than those of medullary bone (i.e., proteoglycans), the crystal growth and recrystallization of bone mineral are delayed in cortical bone. This could be due to the fact that, in cortical bone, collagen is the main organic matrix component, and the mineral is integrated within collagen fibrils. Therefore, until this larger amount of collagen or byproducts is completely lost (at around 600 °C), crystal growth and recrystallization is prevented.

Interestingly, elemental mapping by EDS shows notable changes in the distribution of chemical elements at the crystal surface in both types of bone (Figure 5G–5I). At lower temperatures (up to 600 °C), the chemical composition of apatite crystals is homogeneous on the scale observable with EDX (Figure 5G). However, after recrystallization, Na and Mg diffuse out from the apatite crystal lattice and accumulate on the crystal surfaces in the form of very small Mg-rich nanoparticles (about 20 nm in size). These nanoparticles are made of periclase (MgO), which has been identified by XRD as a minority mineral phase besides apatite (see below and in SI in Figures S9, S10). Periclase formation occurs above 600 °C, and it has been estimated to range from 0.3% at 600 °C to 1.2% at 800 °C (see Supporting Information). Other authors[48] have also described the formation of lime (CaO) in burned bones, but this mineral phase was not detected here. Greiner et al.[7] observed the formation of buchwaldite ($NaCaPO_4$) in bovine bone when treated at 800 °C and above. However, the formation of buchwaldite was not observed in the present study, even though Na diffuses out to the surface of crystals. A lower Na concentration in avian bones could have prevented its formation. All in all, there are not only changes in the size of apatite crystals during heating-induced recrystallization but also changes in their surface chemistry. The recrystallization process is, in fact, a reaction from nanocrystalline Mg-bearing carbonate apatite to highly crystalline hydroxyapatite, where the Mg^{2+} is expelled from the original apatite to the surface of the growing crystal. These changes should modify bone mineral properties, making it more reactive as periclase and/or lime are highly reactive (to CO_2 and water[49]).

X-ray Diffraction: Organic Matrix, Mineral Crystallinity, and Organization. The X-ray diffraction data also

https://doi.org/10.1021/acs.cgd.3c00648
Cryst. Growth Des. XXXX, XXX, XXX–XXX

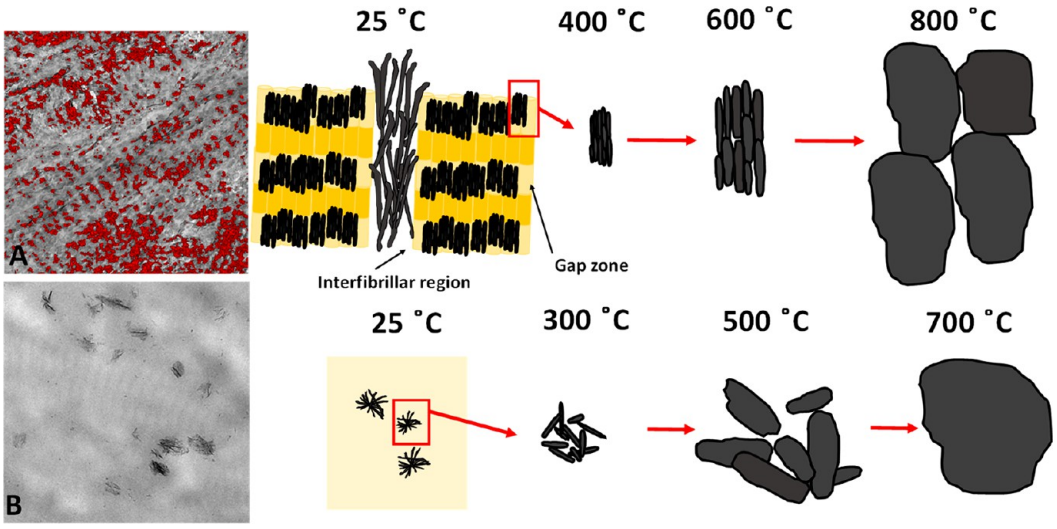

Figure 6. Schematic drawing depicting the transformation of cortical and medullary bone during heating. A) In cortical bone, apatite crystals mineralize collagen fibrils and nucleate in the collagen gap zones (Ca-rich areas in red). The organic matrix is also mineralized by strands of apatite crystals in the interfibrillar regions. With increasing temperature, the organic matter is lost, and the crystal grows in size but preserves the elongated shape and crystal orientation. At higher temperatures, crystals grow very rapidly in all directions and develop a euhedral morphology. B) Medullary bone is mineralized by small apatite crystals forming isolated aggregates. The onset of crystallization occurs at lower temperatures, and crystals grow rapidly in all directions, developing a large size.

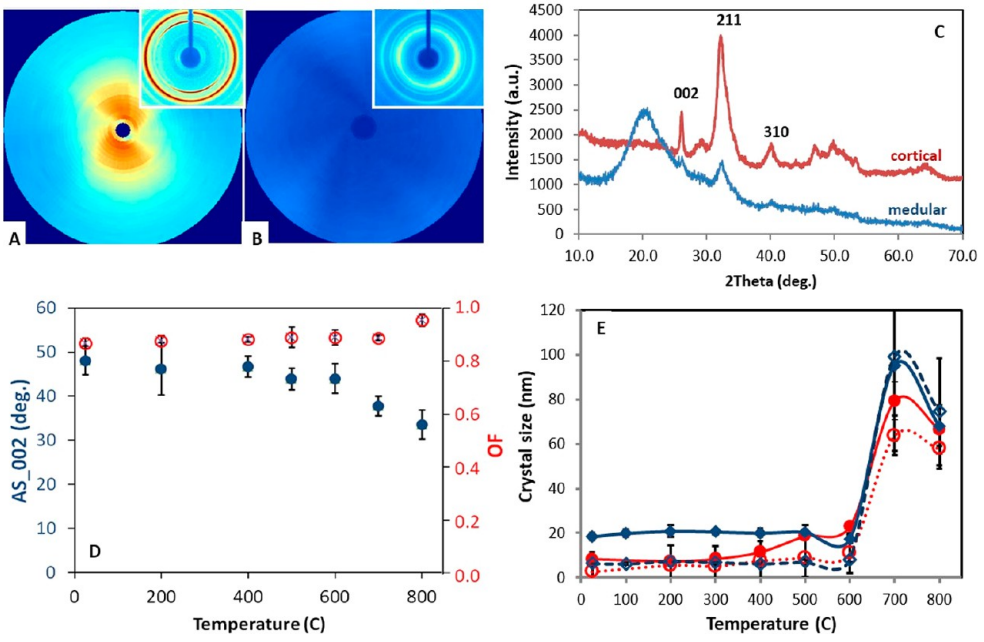

Figure 7. Bone microstructure was analyzed by X-ray diffraction. A, B) Pole figure and 2D-XRD patterns (inset) of (untreated) cortical (A) and medullary (B) bone. C) Theta-2Theta scans of powdered (untreated) bone samples. D) Evolution of crystal orientation with temperature measured as the angular spread of 002 reflections (AS_002) (blue solid circles) and oriented fraction (OF) (red open circles) in cortical bone. E) Evolution of crystallite size with temperature for cortical (diamonds) and medullary (circles) bone. Full markers (solid lines) and open markers (dashed lines) correspond to the crystallite size measured.

show notable differences between cortical and medullary bone. In the case of untreated cortical bone, the 002 pole figure (Figure 7A) shows a unique and broad maximum around the center, indicating that apatite crystals are aligned with their *c*-axis parallel to the elongation of bone, but rotated around it (fiber texture). Even though crystals are preferentially oriented, there is a broad distribution in the orientation of their *c*-axis (about 45−50°), as visible from the diffraction intensities concentrated in 45−50° arcs of the Debye−Scherrer rings due to the preferential orientation of apatite crystals in this tissue (Figure 6A inset). On the other hand, medullary bone produces a pole figure with homogeneous intensity, since apatite crystals are randomly oriented in this tissue. Also, in the associated 2D-XRD pattern, the intensity is constant along the Debye−Scherrer rings as randomly oriented crystals contribute equally in all directions (Figure 7B inset).

1D-XRD (Theta-2Theta) scans of powdered bone samples also show notable differences between cortical and medullary bone (Figures 7C, S9). Both types of bone show a well-defined 002 peak and a broad band (from overlapping 211, 112, and

https://doi.org/10.1021/acs.cgd.3c00648
Cryst. Growth Des. XXXX, XXX, XXX−XXX

300 peaks), due to the nanocrystalline nature of the bone apatite. Cortical bone produces more intense and better defined peaks than medullary bone, due to the slightly greater crystallinity of the first. In both tissues, there is a highly anisotropic peak broadening due to the elongated shape of apatite crystals along their *c*-axis, which produces sharper peaks for the 002 reflection than for other directions (310 peak; *a*- and *b*-axes) (Figure 7C). From the peak broadening of 002 and 310 reflections, the length (along the *c*-axis) and width (along the *a*- and *b*-axes) of apatite crystals in bone were determined. The calculated crystallite size of apatite in cortical bone (19 nm × 6 nm) is larger than that in medullary bone (8 nm × 2 nm). Comparing XRD results with TEM measurements, XRD data reproduce quite well the dimensions of crystals, but show that the crystallite size along the *c*-axis is smaller than the length of the apatite nanoparticles observed by TEM. In any case, XRD data are able to reveal differences in mineral crystallinity between the two types of bones. Additionally, the diffractogram of medullary bone has a broad band at around 20° 2θ (Cu Kα) due to the presence of a large amount of amorphous organic matter in this tissue.

In cortical bone, apatite crystals are preferentially oriented with their *c*-axis parallel to the long axis of the bone, but there is a small fraction of randomly oriented crystals as well. Each differently oriented population of crystals contributes to different parts of the 2D-XRD pattern (e.g., to arcs or the whole Debye−Scherrer ring), making it possible to determine their crystallite size independently.[24] In fact, preferentially oriented apatite crystals are larger (19 nm × 10 nm) than randomly oriented crystals (18 nm × 7 nm), with the most notable differences in their width. The oriented fraction, formed by larger crystals, could be intrafibrillar apatite crystals that nucleate within collagen fibrils or at the surface and are oriented parallel to the fibrils. Smaller randomly oriented apatite nanocrystals could mineralize the interfibrillar region and be more disorganized. Other studies have shown that the size and orientation of apatite varies in intrafibrillar or extrafibrillar regions, with the latter having a lesser degree of crystal orientation.[18,50]

The X-ray diffraction data from the tibiae cortical and medullary bone treated (annealed) at different temperatures show that there are notable changes in bone mineral organization (crystal orientation) and crystallinity (crystal size) with temperature. The 2D-XRD data show that, in cortical bone, the angular spread in the orientation of crystals is nearly constant up to 600 °C and decreases gradually at higher annealing temperatures, from about 45° down to 33° (Figure 6D). Also, there is a slight, but gradual, increase in the oriented fraction from 0.87 to 0.96. These data, all combined, indicate that during recrystallization above 600 °C, the larger, oriented apatite crystals grow at the expense of the smaller, randomly oriented apatite crystals, that act as a template for epitaxial nucleation during an Ostwald ripening process.[46] This process increases the preferred orientation of apatite in the bone mineral.

On the other hand, the XRD data also show that the size of the crystals is nearly constant up to a certain temperature (recrystallization temperature), and above that, there is a rapid increase in the size of crystals due to the recrystallization process (Oswald ripening) (Figure 6E). In cortical bone, the onset of recrystallization occurs at about 600 °C, whereas in medullary bone, this process starts at much lower temperatures (around 400 °C), increasing the crystal size first slowly (below 600 °C) and finally very rapidly (above 600 °C). These results are in agreement with the TEM observations, though direct observation with electron microscopy is able to detect these changes earlier at lower temperatures.

Additionally, XRD data also provide complementary information regarding the structural changes of the bone organic matrix that could not be detected by other analytical techniques (i.e., TGA, FTIR). The organic matrix of untreated cortical bone (25 °C) and cortical bone treated at 100 °C (Figure 8A) shows a characteristic fiber diffraction pattern with

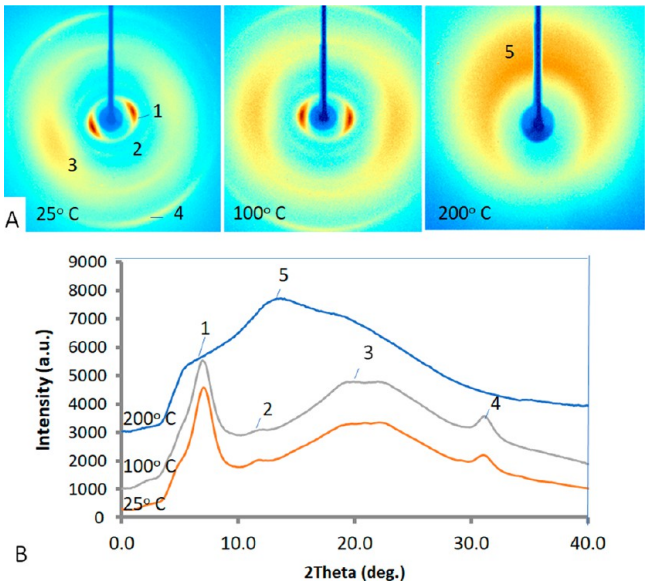

Figure 8. X-ray diffraction analysis of demineralized cortical bone treated at different temperatures. A) 2D-XRD patterns of demineralized untreated bone (25 °C) and bone treated at 100 and 200 °C. B) 1D-2Theta scans of demineralized bone samples treated at different temperatures. Peaks in 2D- and 1D-XRD patterns from collagen (1, 3, and 5) and the mineral part (2 and 4) are indicated by numbers.

two arcs (1 and 3) in the equatorial region, produced by well-oriented collagen fibrils, and two faint arcs (2 and 4) in the meridional region, from the remaining mineral part that has not been completely dissolved. In the 1D-2Theta scans (Figure 8B), peak 1, shown at around 8° (*d* spacing = 1.20 nm), corresponds to the lateral packing of collagen fibrils, and peak 3, shown at around 20° (*d* spacing = 0.45 nm), corresponds to the diffuse scattering of amorphous/unordered regions in collagen molecules.[51,52] Peaks 2 and 4 correspond to apatite reflections from the remaining mineral part that has not been completely dissolved. These data for cortical bone treated at 200 °C (Figure 8B) show a very broad band at around 13° (0.66 nm) due to diffuse scattering, indicating that collagen now has an unordered structure and has been denatured. Still, some features of peak 1 remain, indicating that part of the original collagen structure or molecular arrangement (packing) has been preserved. For cortical bone samples treated at higher temperatures (300 °C and above), after bone demineralization, the remaining organics have no structural integrity and could not be recovered for XRD analyses. On the other hand, the organic matrix of medullary bone (from untreated or treated samples) only produces diffuse scattering, confirming that it has an unordered structure. Thus, it is shown that collagen structure is preserved up to 100 °C, denatures at 200 °C, and is

https://doi.org/10.1021/acs.cgd.3c00648
Cryst. Growth Des. XXXX, XXX, XXX−XXX

completely degraded at 300 °C and above. The XRD results are in agreement with FTIR analysis, though XRD is able to detect structural changes of collagen at a lower temperature than FTIR (200 °C vs 300 °C). In future studies, we will use SAXS to see if we could detect more subtle structural changes (i.e., collagen periodic banding) that could not be detected here, as the beam stop in our XRD system cut the low angle signal (<5°).

In conclusion, there are well-defined changes in bone chemistry, structure, and crystallinity during thermal treatment. Also, the behavior of different types of bone with heating is very different, as the surface properties of these materials and their reactivity are mainly dependent on bone mineral characteristics such as crystallinity, porosity, organic matrix composition, and its structural relationship with the mineral. Thus, cortical bone mineral is integrated within the collagen fibrils and has a large amount of noncollagenous acidic proteins (i.e., osteocalcin, osteopontin) strongly bound to the surface of apatite crystals.[16] Collagen structure denaturation and degradation occur in the low temperature range (up 300 °C). Up to 400 °C, there are notable changes in the mineral part with a gradual conversion of amorphous phosphate into crystalline domains. At higher temperatures (above 600 °C), a significant coarsening of crystals occurs, probably due to an Oswald ripening process. The recrystallization set in when all organics that are intimately associated with the mineral are lost. Medullary bone's greater porosity, lower crystallinity and structural organization, and association with the organic matrix rich in proteoglycans could explain its higher reactivity in response to heating. On the other hand, we show that a strongly textured apatitic ceramic material can be produced from cortical bone, or a highly porous apatitic ceramic material from medullary bone. The latter could be similar to commercial coralline hydroxylapatite used as bone graft substitute made from sea corals (*Porites sp.*) that have also a large porosity.[53] Also, the latter could be used as filters or in chromatography as apatite has a strong affinity to proteins. Therefore, relevant microstructure characteristics (porosity, crystal size, morphology, and surface properties) can be modified in a controlled way by first selecting the type of bone and then adjusting the treatment temperature. The properties and performance of polycrystalline ceramic materials can be enhanced by increasing the preferential orientation of crystals by texturing that eliminates high-angle grain boundaries. These materials can behave like single crystals (for a directional property of interest like, e.g., ionic conduction) but at the same time have the mechanical robustness of polycrystalline ceramics.[46] Even though in this study we used avian bone, avian cortical bone has a very similar chemical composition and structural organization to that of mammalian bone, so these results could be applied also to understand mammalian bone transformation during heating. Medullary bone, though structurally and chemically very different, has the same mineral composition and is an interesting model to understand the influence of the organic matrix on mineral transformation.

■ ASSOCIATED CONTENT

Supporting Information

The Supporting Information is available free of charge at https://pubs.acs.org/doi/10.1021/acs.cgd.3c00648.

Transmission electron microscopy images; Infrared spectroscopy peak fitting and compositional parameters; X-ray diffraction at different temperatures (PDF)

■ AUTHOR INFORMATION

Corresponding Author

Alejandro B. Rodríguez Navarro − *Departamento de Mineralogía y Petrología, Universidad de Granada, 18002 Granada, Spain;* orcid.org/0000-0003-2674-7383; Email: anava@ugr.es

Authors

Sergio Madero − *Departamento de Mineralogía y Petrología, Universidad de Granada, 18002 Granada, Spain*

Martina Greiner − *Department für Geo- und Umweltwissenschaften, Ludwig-Maximilians-Universität, 80333 Munich, Germany;* orcid.org/0000-0003-4843-3043

Pablo A. Rodriguez-Jimenez − *Departamento de Mineralogía y Petrología, Universidad de Granada, 18002 Granada, Spain*

Wolfgang W. Schmahl − *Department für Geo- und Umweltwissenschaften, Ludwig-Maximilians-Universität, 80333 Munich, Germany*

Concepción Jiménez-López − *Departamento de Microbiología, Universidad de Granada, 18002 Granada, Spain;* orcid.org/0000-0002-5645-2079

Complete contact information is available at: https://pubs.acs.org/10.1021/acs.cgd.3c00648

Notes

The authors declare no competing financial interest.

■ ACKNOWLEDGMENTS

We thank funding through grants from Junta de Andalucía (P20_00208 and P20_00207) and the Spanish government (PID2020-116660GB-I00), UCE-PP2016-05, and the Biotechnology Institute (University of Granada). We also thank Ma Jose Martinez, Cecilia de la Prada (CIC - University of Granada) for technical assistance with the TEM analyses.

■ REFERENCES

(1) Shipman, P.; Foster, G.; Schoeninger, M. Burnt bones and teeth: an experimental study of color, morphology, crystal structure and shrinkage. *Journal of Archaeological Science* **1984**, *11* (4), 307−325.

(2) Stiner, M. C.; Kuhn, S. L.; Weiner, S.; Bar-Yosef, O. Differential Burning, Recrystallization, and Fragmentation of Archaeological Bone. *Journal of Archaeological Science* **1995**, *22* (2), 223−237.

(3) Weiner, S.; Bar-Yosef, O. States of preservation of bones from prehistoric sites in the Near East: a survey. *J. Archeol. Sci.* **1990**, *17*, 187−196.

(4) Berna, F.; Matthews, A.; Weiner, S. Solubilities of bone mineral from archeological sites: the recrystallization window. *J. Archaeol. Sci.* **2004**, *31*, 867−882.

(5) Etok, S. E.; Valsami-Jones, E.; Wess, T. J.; Hiller, J. C.; Maxwell, C. A.; Rogers, K. D.; Manning, D. A. C.; White, M. L.; Lopez-Capel, E.; Collins, M. J.; Buckley, M.; Penkman, K. E. H.; Woodgate, S. L. Structural and chemical changes of thermally treated bone apatite. *J. Mater. Sci.* **2007**, *42*, 9807−9816.

(6) Beasley, M. M.; Bartelink, E. J.; Taylor, L.; Miller, R. M. Comparison of transmission FTIR, ATR, and DRIFT spectra: implications for assessment of bone bioapatite diagenesis. *Journal of Archaeological Science* **2014**, *46*, 16−22.

(7) Greiner, M.; Rodríguez-Navarro, A.; Heinig, M. F.; Mayer, K.; Kocsis, B.; Göhring, A.; Toncala, A.; Grupe, G.; Schmahl, W. W. Bone incineration: An experimental study on mineral structure, colour and crystalline state. *Journal of Archaeological Science: Reports* **2019**, *25*, 507−518.
(8) Marques, M. P. M.; Batista de Carvalho, L. A. E.; Gonçalves, D.; Cunha, E.; Parker, S. F. The impact of moderate heating on human bones: an infrared and neutron spectroscopy study. *R Soc. Open Sci.* **2021**, *8* (10), No. 210774.
(9) Nakano, T.; Fujitani, W.; Umakoshi, Y. Synthesis of Apatite Ceramics with Preferential Crystal Orientation. *Mater. Sci. Forum* **2004**, *449*−*452*, 1289−1292.
(10) Figueiredo, M.; Cunha, S.; Martins, G.; Freitas, J.; Judas, F.; Figueiredo, H. Influence of hydrochloric acid concentration on the demineralization of cortical bone. *Chem. Eng. Res. Des.* **2011**, *89*, 116−124.
(11) Sneddon, I. R.; Orueetxebarria, M.; Hodson, M. E.; Schofield, P. F.; Valsami-Jones, E. Use of bone meal amendments to immobilize Pb, Zn and Cd in soil: a leaching column study. *Environ. Pollut.* **2006**, *144*, 816−825.
(12) Li, X.; Van Blitterswijk, C. A.; Feng, Q.; Cui, F.; Watari, F. The effect of calcium phosphate microstructure on bone-related cells in vitro. *Biomaterials* **2008**, *29*, 3306−3316.
(13) Weiner, S.; Wagner, H. D. The material bone: Structure-Mechanical Function Relations. *Annu. Rev. Mater. Sci.* **1998**, *28*, 271−298.
(14) Fratzl, P.; Gupta, H. S.; Paschalis, E. P.; Roschger, P. Structure and mechanical quality of the collagen-mineral nano-composite in bone. *J. Mater. Chem.* **2004**, *14*, 2115−2123.
(15) Schmahl, W. W.; Kocis, B.; Toncala, A.; Grupe, G. J. Mineralogic characterization of archaeologic bone. In *Isotopic landscapes in bioarchaelogy*; Grupe, G., McGlynn, G. C., Eds., Springer: Berlin, Germany, 2016, pp 17−41. .
(16) Stock, S. R. The Mineral−Collagen Interface in Bone. *Calcified Tissue International* **2015**, *97* (3), 262−280.
(17) Macias-Sánchez, E.; Tarakina, N. V.; Ivanov, D.; Blouin, S.; Berzlanovich, A. M.; Fratzl, P. Spherulitic Crystal Growth Drives Mineral Deposition Patterns in Collagen-Based Materials. *Adv. Funct. Mater.* **2022**, *32*, No. 2200504.
(18) Grünewald, T. A.; Liebi, M.; Wittig, N. K.; Johannes, A.; Sikjaer, T.; Rejnmark, L.; Gao, Z.; Rosenthal, M.; Guizar-Sicairos, M.; Birkedal, H.; Burghammer, M. Mapping the 3D orientation of nanocrystals and nanostructures in human bone: Indications of novel structural features. *Sci. Adv.* **2020**, *6*, No. eaba4171.
(19) Boskey, A. L.; Spevak, L.; Paschalis, E.; Doty, S. B.; McKee, M. D. Osteopontin deficiency increases mineral content and mineral crystallinity in mouse bone. *Calcif. Tissue Int.* **2002**, *71*, 145−154.
(20) Hu, Y.-Y.; Rawal, A.; Schmidt-Rohr, K. Strongly bound citrate stabilizes the apatite nanocrystals in bone. *Proc. Natl. Acad. Sci. U. S. A.* **2010**, *107* (52), 22425.
(21) Landis, W. J.; Jacquet, R. Association of calcium and phosphate ions with collagen in the mineralization of vertebrate tissues. *Calcif Tiss Int.* **2013**, *93*, 329−337.
(22) Davies, E.; Müller, K. H.; Wong, W. C.; Pickard, C. J.; Reid, D. G.; Skepper, J. N.; Duer, M. J. Citrate bridges between mineral platelets in bone. *Proc. Natl. Acad. Sci. U. S. A.* **2014**, *111* (14), E1354−E1363.
(23) Delgado-Lopez, J. M.; Iafisco, M.; Rodriguez, I.; Tampieri, A.; Prat, M.; Gomez-Morales, J. Crystallization of bioinspired citrate-functionalized nanoapatite with tailored carbonate content. *Acta Biomater.* **2012**, *8*, 3491−3499.
(24) Dominguez-Gasca, N.; Benavides-Reyes, C.; Sanchez-Rodriguez, E.; Rodriguez-Navarro, A. B. Changes in avian cortical and medullary bone mineral composition and organization during acid-induced demineralization. *Eur. J. Mineral.* **2019**, *31*, 209−216.
(25) Donnelly, E.; Boskey, A. L.; Baker, S. P.; Van der Meulen, M. C. Effects of tissue age on bone tissue material composition and nanomechanical properties in the rat cortex. *J. Biomed Mater. Res. A* **2009**, *92* (3), 1048−1056.
(26) Benavides-Reyes, C.; Rodriguez-Navarro, A. B.; McCormack, H. A.; Eusemann, B. K.; Dominguez-Gasca, N.; Alvarez-Lloret, P.; Fleming, R. H.; Petow, S.; Dunn, I. C. Comparative analysis of the morphology, chemistry and structure of the tibiotarsus, humerus and keel bones in laying hens. *Br Poult Sci.* **2021**, *62* (6), 795−803.
(27) Ascenzi, A.; Francois, C.; Bocciarelli, D. S. On the bone induced by oestrogens in birds. *J. Ultrastruct. Res.* **1963**, *8*, 491−505.
(28) Bonucci, E.; Gherardi, G. Histochemical and electron microscope investigations on medullary bone. *Cell Tissue Res.* **1975**, *163* (1), 81−97.
(29) Rodriguez-Navarro, A. B.; McCormack, H. M.; Fleming, R. H.; A lvarez-Lloret, P.; Romero-Pastor, J.; Dominguez Gasca, N.; Prozorov, T.; Dunn, I. Influence of physical activity on tibial bone material properties in laying hens. *J. Struct. Biol.* **2018**, *201*, 36−45.
(30) Van de Velde, J. P.; Vermeiden, J. P. W.; Bloot, A. M. Medullary bone matrix formation mineralization and remodeling related to dialy egg-laying cycle of Japanese quail: a histological and radiological study. *Bone* **1985**, *6*, 321−328.
(31) Kerschnitzki, M.; Zander, T.; Zaslansky, P.; Fratzl, P.; Shahar, R.; Wagermaier, W. Rapid alterations of avian medullary bone material during the daily egg-laying cycle. *Bone* **2014**, *69*, 109−117.
(32) Stringer, D. A.; Taylor, T. G. The calcification mechanism as exemplified by a histochemical study of avian medullary bone. *Biochem. J.* **1961**, *78*, 19.
(33) Eusemann, B. K.; Ulrich, R.; Sanchez-Rodriguez, E.; Benavides-Reyes, C.; Dominguez-Gasca, N.; Rodriguez-Navarro, A. B.; Petow, S. Bone quality and composition are influenced by egg production, layer line, and oestradiol-17ß in laying hens. *Avian Pathol.* **2022**, *51* (3), 267−282.
(34) Fleming, R. H.; McCormack, H. A.; Mcteir, L.; Whitehead, C. C. Relationships between Genetic, Environmental and Nutritional Factors Influencing Osteoporosis in Laying Hens. *British Poultry Science* **2006**, *47* (6), 742−755.
(35) Ellingham, S. T. D.; Thompson, T. J. U.; Islam, M. Thermogravimetric analysis of porperty changes and weight loss in incinerated bone. *Palaeogeogr. Palaeoclimatol. Palaeoecol.* **2015**, *438*, 239−244.
(36) Lim, J. J.; Shamos, M. H. Evaluation of kinetic parameters of thermal decomposition of native collagen by thermogravimetric analysis. *Biopolymers* **1974**, *13*, 1791−807.
(37) Snowden, J. M. The stabilization of in vivo assembled collagen fibrils by proteoglycans/glycosaminoglycans. *Biochim. Biophys. Acta* **1982**, *703* (1), 21−25.
(38) Konovalova, I.; Novikov, V.; Kuchina, Y.; Dolgopiatova, N. Technology and Properties of Chondroitin Sulfate from Marine Hydrobionts. *International applied research conference Biological Resources Development and Environmental Management, KnE Life Sciences* **2020**, 305−314.
(39) Rey, C.; Shimizu, M.; Collins, B.; Glimcher, M. J. Resolution-enhanced fourier transform infrared spectroscopy study of the environment of phosphate ions in the early deposits of a solid phase of calcium-phosphate in bone and enamel, and their evolution with age. I: Investigations in the v4 PO4 domain. *Calcif Tissue Int.* **1990**, *46*, 384−394.
(40) Rey, C.; Combes, C.; Drouet, C.; Glimcher, M. J. Bone mineral: update on chemical composition and structure. *Osteoporos Int.* **2009**, *20* (6), 1013−1021.
(41) Mahamid, J.; Sharir, A.; Addadi, L.; Weiner, S. Amorphous calcium phosphate is a major component of the forming fin bones of zebrafish: Indications for an amorphous precursor phase. *Proc. Natl. Acad. Sci. U. S. A.* **2008**, *105* (35), 12748−12753.
(42) LeGeros, R. Z. Formation and transformation of calcium phosphates: relevance to vascular calcification. *Z. Kardiol.* **2001**, *90* (15), 116−124.
(43) Kubisz, L.; Mielcarek, S. Differential scanning calorimetry and temperature dependence of electric conductivity in studies on denaturation process of bone collagen. *J. Non-Cryst. Solids* **2005**, *351*, 2935−2939.

https://doi.org/10.1021/acs.cgd.3c00648
Cryst. Growth Des. XXXX, XXX, XXX−XXX

(44) Ferreira, A. M.; Noris-Suarez, K.; Ciardelli, G. The Influence of Proteoglycans on Collagen Properties. *5th Freiberg Collagen Symposium*; Forschungsinstitut für Leder und Kunstaffbahnen (FILK) gGmbH, 2012.
(45) Lambri, M. L.; Giordano, E. D.; Bozzano, P. B.; Bonifacich, F. G.; Pérez-Landazábal, J. I.; Zelada, G. I.; Gargicevich, D.; Recarte, V.; Lambri, O. A. Thermal Degradation of Type I Collagen from Bones. *Journal of Renewable Materials* **2016**, *4* (4), 251−257.
(46) Messing, G. L.; Poterala, S.; Chang, Y.; Frueh, T.; Kupp, E. R.; Watson, B. H.; Walton, R. L.; Brova, M. J.; Hofer, A.-K.; Bermejo, R.; Meyer, R. J. Texture-engineered ceramics—Property enhancements through crystallographic tailoring. *J. Mater. Res.* **2017**, *32* (17), 3219−3241.
(47) Fujisawa, R.; Tamura, M. Acidic bone matrix proteins and their roles in calcification. *Front Biosci (Landmark Ed)* **2012**, *17* (5), 1891−1903.
(48) Piga, G.; Thompson, T. J. U.; Malgosa, A.; Enzo, S. The potential of X-ray diffraction in the analysis of burned remains from forensic contexts. *J. Forensic Sci.* **2009**, *54*, 534−539.
(49) Rodriguez-Navarro, C.; Ruiz-Agudo, E. Nanolimes: from synthesis to application. *Pure Appl. Chem.* **2018**, *90* (3), 523−550.
(50) Hassenkam, T.; Fantner, G. E.; Cutroni, J. A.; Weaver, J. C.; Morse, D. E.; Hansma, P. K. High-resolution AFM imaging of intact and fractured trabecular bone. *Bone* **2004**, *35*, 4−10.
(51) Cameron, G. J.; Alberts, I. L.; Laing, J. H.; Wess, T. J. Structure of type I and type III heterotypic collagen fibrils: an X-ray diffraction study. *J. Struct. Biol.* **2002**, *137* (1−2), 15−22.
(52) Wu, B.; Mu, C.; Zhang, G.; Lin, W. Effects of Cr3+ on the Structure of Collagen Fiber. *Langmuir* **2009**, *25* (19), 11905−11910.
(53) Roy, D.; Linnehan, S. Hydroxyapatite formed from Coral Skeletal Carbonate by Hydrothermal Exchange. *Nature* **1974**, *247*, 220−222.

https://doi.org/10.1021/acs.cgd.3c00648
Cryst. Growth Des. XXXX, XXX, XXX−XXX